Applied Catalysis B: Environmental 147 (2014) 973–979

Contents lists available at ScienceDirect

Applied Catalysis B: Environmental

journal homepage: www.elsevier.com/locate/apcatb

Nano TiO_2-functionalized magnetic-cored dendrimer as a photocatalyst

Lyung-Joo Kim, Jun-Won Jang, Jae-Woo Park*

Department of Civil and Environmental Engineering, Hanyang University, 222 Wangsimni-ro, Seongdong-gu, Seoul 133-791, South Korea

ARTICLE INFO

Article history:
Received 8 May 2013
Received in revised form 7 October 2013
Accepted 12 October 2013
Available online 19 October 2013

Keywords:
Dendrimer
Titanium dioxide
Magnetite
Methyl orange
Electron transfer

ABSTRACT

Nano-sized TiO_2 terminals were linked with magnetic-cored dendrimers by a divergent method in this research. Significant improvement in photocatalytic activity was monitored in decolorization of methyl orange (MO) in comparison with bare nano TiO_2 and Fe/Ti mixture at the same ratio. Enhanced photocatalytic activity of magnetic-cored dendrimers with nano-sized TiO_2 (TD) can be attributed to restrained recombination of electron–hole pairs because of photoexcited electron capture in dendrimers. MO decolorization was facilitated by synergistic effect from surface adsorption and photocatalytic activity. Experimental results were fitted well with the Langmuir–Hinshelwood (L–H) model, which indicated that the photodecolorization after adsorption. The observed decolorization rate constant and the adsorption coefficient values were 0.0478 and 0.0812, respectively. Reuse of TD was also investigated for five successive runs.

1. Introduction

Titanium dioxide (TiO_2) photocatalyst is widely used in a variety of applications including air/water treatment, hydrogen evolution, sterilization, and so on [1–4]. Nano TiO_2 also shows high photocatalytic activity as it has high sensitivity to light and large specific surface area [1–3]. Nano TiO_2-based photocatalytic degradation of organic compounds, such as methyl orange (MO) [4,5], methylene blue [6,7], humic acid [8,9], and so on, has been well reported. However, applications of TiO_2 of all sizes are limited due to recovery, dispersion, high recombination rate of photo-induced electron–hole pairs, and so on. Some have tried to overcome the aforementioned limitations. For instance, magnetically separable photocatalysts of $TiO_2/SiO_2/Fe_3O_4$ nanoparticles were suggested in order to improve the recovery from treated water [10–12]. Nakanish et al. [13,14] reported that dendrimers prevented TiO_2 nanoparticles from agglomeration by forming a protective sphere.

Dendrimers are highly branched macromolecules with well-defined composition and structure [15,16]. They are built up of three-dimensional architecture, "branch cells" that are organized in concentric layers around a core [17]. They can be divided into three main components: a core, interior branch cells, and terminal branch cells which can be functionalized. For this reason, the overall chemical and physical properties of dendrimers can be configured to specific needs by changing the terminal branch cells at outermost generation [18]. Due to their structural features, dendrimers have been widely applied in many fields including biomaterial, biomedicine, targeting carrier, therapeutic treatment of cancer cell, catalysis, drug delivery, and so on [19–24]. Some recent studies include environmental applications. For example, Diallo et al. [25] investigated the removal of copper from water using various generation of poly amidoamine (PAMAM) dendrimers with ethylene diamine core and terminal NH_2 groups. Magnetite-cored dendrimers with an advantage of easy magnetic separation were also proposed for heavy metal uptake from water [26,27].

In this research, we report the synthesis of magnetic-cored dendrimers with TiO_2 terminal groups for possible applications in water treatment, solar cells, and so on. We hypothesized that this new material can aid: (i) enhanced recovery from treated water using magnetic force, (ii) better dispersion of TiO_2 nanoparticles due to the incorporation of them into dendrimer structure, and (iii) photo-induced electron transfer from TiO_2 to magnetic-cored dendrimer. Therefore, the objective of this study was to experimentally test the three hypotheses in photocatalytic decolorization of MO.

2. Experimental

2.1. Materials

MO, $C_{14}H_{14}N_3SO_3Na$, was obtained from Sigma-Aldrich (USA). TiO_2 powder (Degussa P25) with mainly anatase (80%),

* Corresponding author. Tel.: +82 2 2220 1483/+82 11 9881 2831; fax: +82 2 2220 4322.
E-mail address: jaewoopark@hanyang.ac.kr (J.-W. Park).

0926-3373/$ – see front matter © 2013 Elsevier B.V. All rights reserved.
http://dx.doi.org/10.1016/j.apcatb.2013.10.024

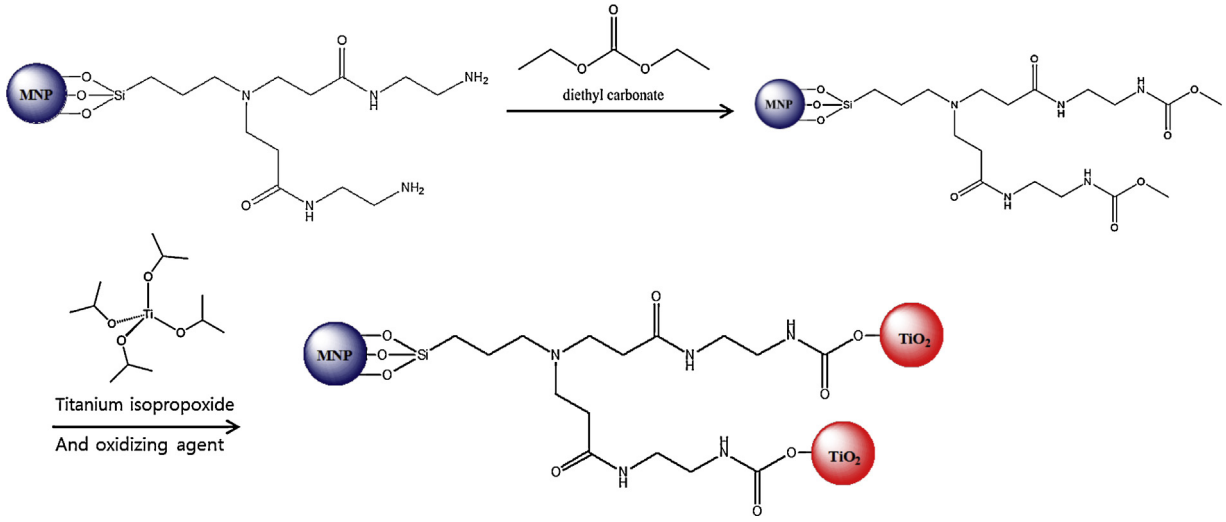

Fig. 1. Schematic of the photoresponsible magnetic-cored dendrimerin this research (TD).

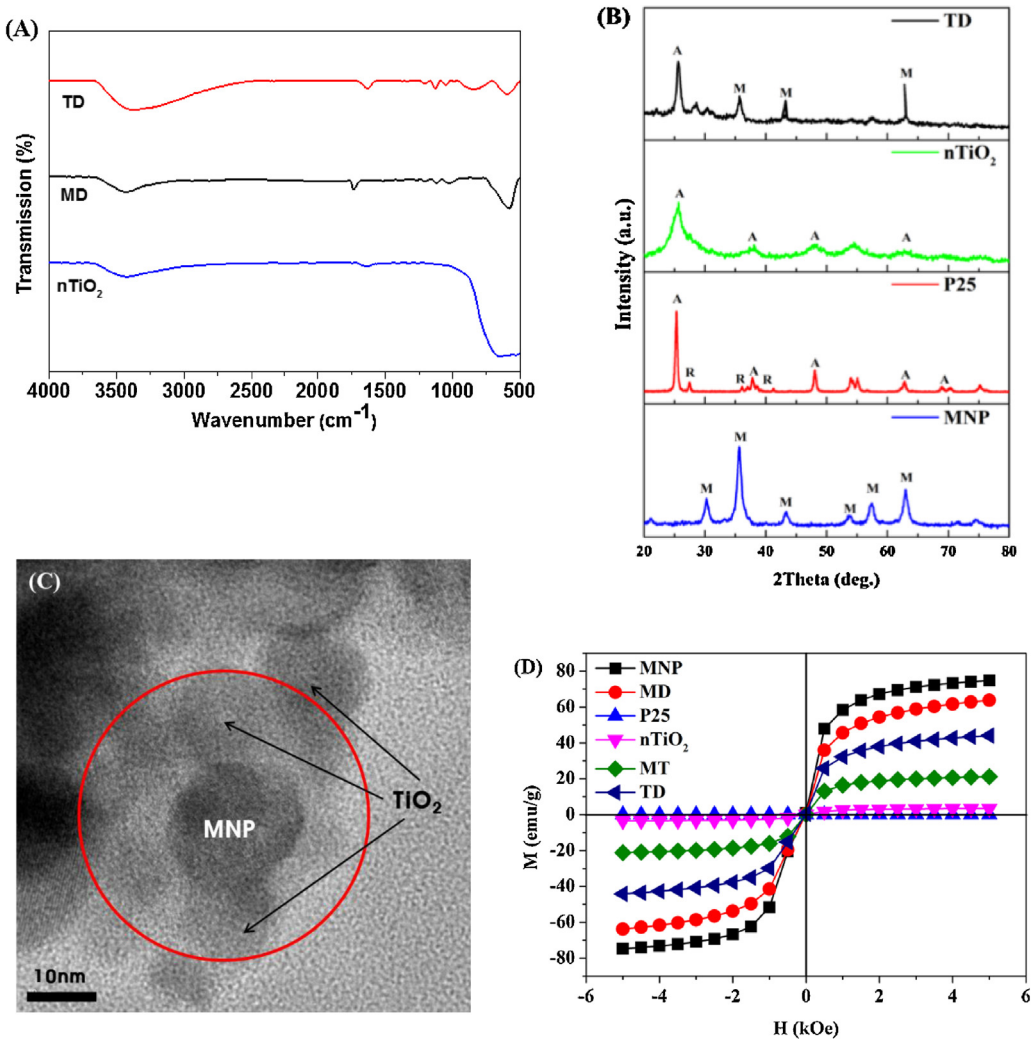

Fig. 2. (A) FT-IR, (B) XRD, (C) TEM, (D) magnetization curves of the MNP, MD, P25, $nTiO_2$, MT, TD measured using SQUID under external magnetic fields (H) from −5 to 5 kOe of TD.

average particle size of 30 nm, and surface area of 50 m^2/g, was purchased from Degussa AG (Germany). Ferrous sulfate heptahydrate ($FeSO_4{\cdot}7H_2O$), 3-aminopropyltrimethoxysilane (APT, $H_2N(CH_2)_3Si(OCH_3)_3$), and titanium (IV) isopropoxide ($C_{12}H_{28}O_4Ti$) were obtained from Sigma-Aldrich (USA). Ferric chloride hexahydrate ($FeCl_3{\cdot}6H_2O$) and methyl acrylate ($CH_2CHCOOCH_3$) were purchased from Junsei (Japan). Ammonium hydroxide ($NH_3{\cdot}H_2O$) and diethyl carbonate (DEC, $C_5H_{10}O_3$) were purchased from Daejung Chemical (Korea). Ethylenediamine ($NH_2CH_2CH_2NH_2$), sulfuric acid (H_2SO_4), and methanol (CH_3OH) were from Kanto Chemical (Japan) and Duksan Chemical (Korea), respectively. Double distilled and deionized water was used throughout the work. All chemicals were reagent grade or above and used without further treatment.

2.2. Synthesis of magnetic-cored dendrimer with TiO_2 (TD)

Magnetic nanoparticles (MNP) were synthesized by coprecipitation of Fe(III) chlorides and Fe(II) sulfate (Fe^{III}/Fe^{II} ratio = 2) with $NH_3{\cdot}H_2O$ [28]. The products were washed with deionized water and methanol after the reaction. Twelve gram of the as-synthesized MNP methanol suspension was stirred with 57.88 mL of APT for 7 h at 60 °C. The products were washed with methanol and deionized water several times. Dendrimer of generation 0 (G0) represents the as-synthesized magnetite nanoparticles modified only with APT. Ten gram of G0 was dispersed in 500 mL methanol and 100 mL methyl acrylate. The suspension was ultrasonicated and stirred at room temperature for 7 h. The particles were washed with methanol 5 times, and then the suspension was stirred at room temperature for 3 h after 20 mL ethylenediamine was added. Methylacrylate and ethylenediamine were added for dendrimer branches to be linked onto the MNP surface [29,30]. The synthesized magnetic-cored dendrimers (MD) were stored in methanol after five times of rinsing with methanol and deionized water.

Amide terminals of MD were converted to TiO_2 groups to attain photoresponsible magnetic-cored dendrimers in this research (Fig. 1). The MDs were dispersed in 200 mL methanol with 100 mL DEC as inorganic binder. The suspension was sonicated for 30 min and stirred at 60 °C for 6 h, and then washed with methanol 3 times. Subsequently, 80 mL titanium(IV) isopropoxide was added into pre-synthesized solution in a Teflon container for solvothermal process. The Teflon container under stainless steel reactor was placed in furnace at 100 °C for 12 h, after which 38.8 mL of concentrated H_2SO_4 (95%) dissolved in 180 mL water was added and kept at 60 °C [31]. The resultant product was washed with deionized water five times and further dried in a vacuum oven at 60 °C. Nano TiO_2 ($nTiO_2$) was prepared in the same process only without MD. Some MNP and $nTiO_2$ were physically mixed together at the same ration of iron and titanium in TD for comparison purpose (MT).

2.3. Characterization

Fourier transform-infrared spectra (FT-IR) of the samples were recorded on a Nicolet Magna-IR 760 ESP spectrometer (Thermo, USA) from 4000 to 400 cm^{-1} with KBr as the reference sample. Measurements were done in transmission mode with spectroscopic grade KBr pellets for powders. Crystal structure of the samples was characterized using a X-ray diffractometer (XRD, Rigaku D/MAX RINT 2000, Japan) with Cu $K\alpha$ radiation (λ = 1.5418740 Å) as X-ray source, operated at 40 kV and 100 mA in the range of 2θ = 20–80°. Morphology of the TD was analyzed using transmission electron microscopy (TEM, JEM-2010, JEOL, Japan) with an accelerating voltage of 16 kV. The TEM samples were prepared by dispersing in ethanol and then dropping the suspension on carbon–copper grids. Energy dispersive spectrum was equipped with a TEM detector

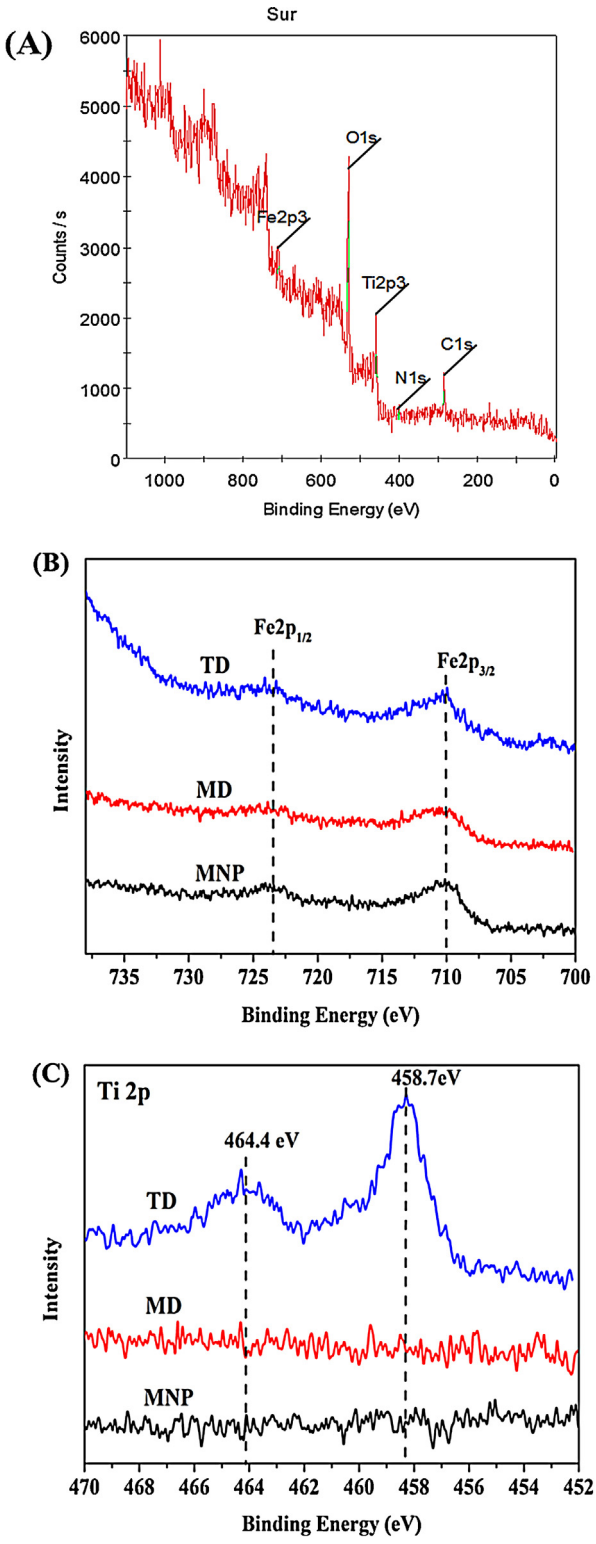

Fig. 3. XPS spectra of TD (A) high resolution survey, (B) Fe, (C) Ti.

for elemental analysis. X-ray photoelectron spectroscopy (XPS, VG Multilab 2000, Thermo VG Scientific, United Kingdom) was used and the X-ray source (Al $K\alpha$, 1253.6 eV) was operated at 10 kV and 30 mA. Atomic force microscopy (AFM, XE-100, PSIA, South Korea) was performed at room temperature. Magnetic properties along with unpaired electrons from oxygen vacancies in TiO_2 crystals were measured with a superconducting quantum interference device (SQUID, MPMS-XL model, Quantum design, USA)

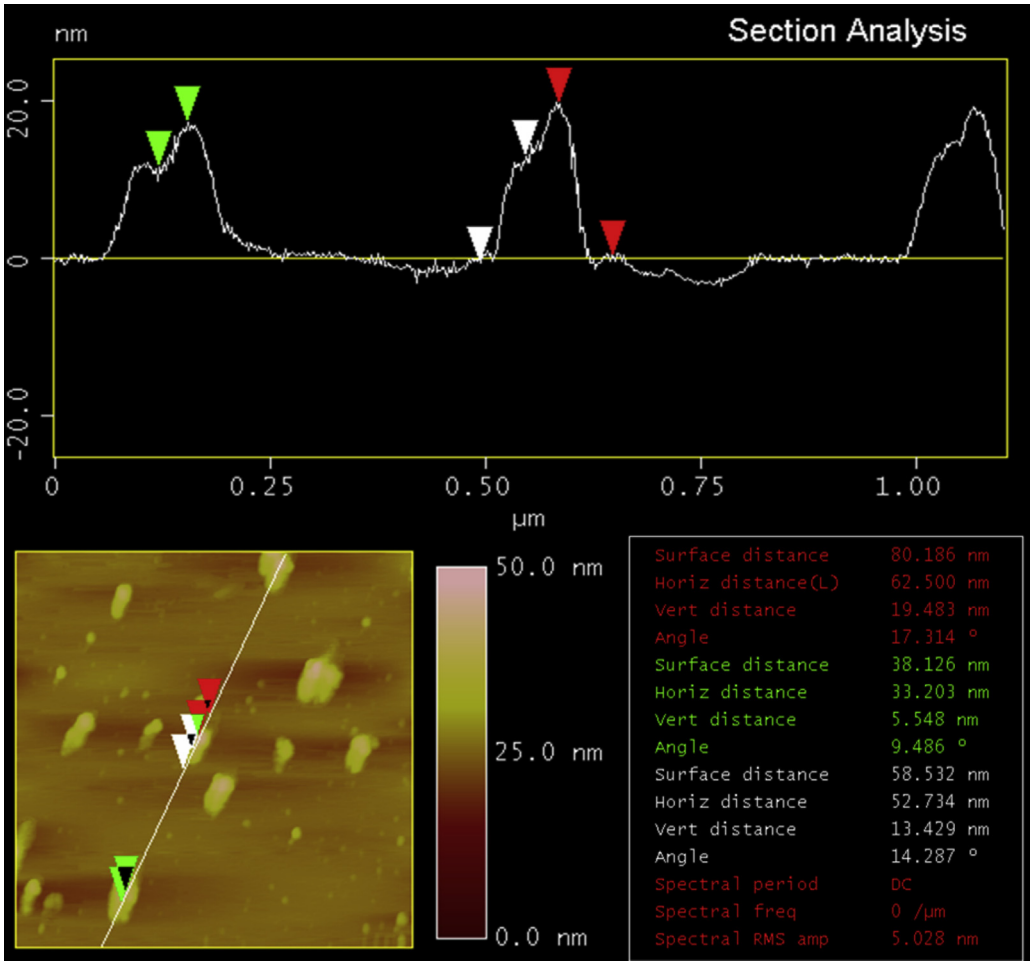

Fig. 4. AFM images of TD.

[32,33]. The specific surface area (BET) of TD was measured with a Micromeritics ASAP 2020 instrument, using the adsorption of N_2 at the temperature of liquid nitrogen (77 K). The fluorescence spectra and lifetime was measured using a fluorescence spectrophotometer (Scinco, FluoroMate FS-2) with a 150 W Xe lamp. Excitation and emission slit width and scan rate were kept constant at 10 nm and 600 nm/min, respectively. Photoluminescence (PL) spectra were obtained at room temperature using a closed-cycle liquid helium cryogenerator (APD, SH-4, USA), a spectrometer (f = 0.5 m, Acton Research Co., Spectrograph 500i, USA), and an intensified photo diode array detector (Princeton Instrument, IR Y1024, USA). A He–Cd laser (Kimon, 1K, Japan) with a wavelength of 325 nm was used as an excitation light source.

2.4. Photocatalytic decolorization and reusability

Photocatalytic decolorization experiments were carried out in a quartz column reactor with maximum volume of 1.5 L. Four 6 W UV-C lights with a radiant wavelength of 254 nm (Philips, USA) were used as ultraviolet light source. The distance between the UV lamps and the quartz reactor was 15 mm. Five hundred mL aqueous MO solution at 10 mg/L was added to the reactor with 0.5 g of catalyst samples. To determine the adsorption constants, different MO concentrations were used. After certain time intervals, 1.5 mL aliquots were sampled and separated magnetically to remove the nanoparticles. The MO samples were analyzed with a UV spectrophotometer (Shimadzu UV-mini 1240, Japan) equipped with a UV detector at 254 nm.

Reusability of TD catalysts was tested in five cycles of repetitive decolorization experiments with initial MO at 3 mg/L and 0.5 g TD. After each cycle, the UV light was turned off and TD was separated with a magnet. The photocatalytic reactor was rinsed with deionized water, which was then replenished with fresh MO aqueous solution. The recovered TD was regenerated by washing with distilled water three times.

3. Results and discussion

3.1. TD characterization

FT-IR spectra of MD, nTiO_2, and TD are shown in Fig. 2(A). Several characteristic peaks of TD were observed, confirming successful modification of MD to TD. The banding vibration of $-NH_2$ group is seen at 3440 cm^{-1} [29] and the stretching vibration of C=O is found at 1732 cm^{-1} [34]. The band at 2363 cm^{-1} is CO_2 that comes from ambient air [35]. The absorption bands at 1096.9 and 1010.1 cm^{-1} are due to Si–O–Si and Si–O–Fe [36–39], which confirms the aminosilanization reaction was successfully achieved. The characteristic absorption band of Fe–O bond is at 579 cm^{-1} [34,40]. A new peak at 987 cm^{-1} corresponds to stretching of Ti–O–C [41], indicating that TiO_2 is chemically bonded to the terminals of MD. The bending mode of Ti–O groups corresponds to the characteristic peak of TiO_2 at 420–800 cm^{-1} [35], indicating successful combination of MD and TiO_2.

Fig. 2(B) shows the XRD spectra of TD, nTiO_2, P25, and MNP in this research. Relevant peaks of TD were observed in the spectra of

both anatase crystal and magnetite, which indicated that TD had photocatalytic and magnetic properties. Diffraction of Degussa P25 TiO_2 indicates the presence of anatase (JCPDS File no. 21-1272) and to a lesser extent rutile (JCPDS File no. 21-1276), as in the composition given by the manufacturer (80% anatase and 20% rutile). XRD patterns of the MNP used as a seed for dendrimer in this research match well with the standard patterns for bulk magnetite (JCPDS File no. 19-0629). The TD in this research is also confirmed to contain Fe and Ti as shown in Fig. 3(A) in Supporting Information. Fig. 3(B) shows the XPS pattern of $Fe2p_{3/2}$ and $Fe2p_{1/2}$ peaks at 710.1 and 723 eV, respectively. These binding energies are the same as those of $Fe2p_{3/2}$ and $Fe2p_{1/2}$ in magnetite [42,43]. Ti2p exhibited a narrow peak at about 458.7 eV and a broad peak at about 464.4 eV, which is the characteristic of TiO_2 as shown in Fig. 3(C) [44,45].

Fig. 2(C) shows the TEM image of TD. MDs with a diameter of about 14 nm were connected with TiO_2 nanoparticles of bright globular shape. The average diameter of the TDs is estimated as 20–25 nm. Structural morphology of TD is revealed using three-dimensional AFM images in which the average TD size is calculated as 19 nm (Fig. 4). Deposition of $nTiO_2$ (distance between green marks) and MD particles (distance between white marks) produced approximately 6 and 13 nm in height, respectively.

Hysteresis loops of the samples with external magnetic field changed from −5 to 5 kOe at room temperature are in Fig. 2(D). Magnetization values of MNP, MD, and TD were estimated as 74.5, 62.8 and 43.4 emu/g, respectively. Magnetization values of the polymer-covered MNPs are much lower that of bare MNP. Magnetization value of MT was much smaller. Note that TD and MT exhibit different magnetization despite the same ratio of iron and titanium. Magnetization curve of TD, MT were close to the origin, indicating that TD, MT exhibit superparamagnetic properties at room temperature. With superparamagnetic property, TD can be recovered efficiently by magnetic field and easily redispersed in aqueous solution. The specific surface area (BET) of TD was measured with a Micromeritics ASAP 2020 instrument, using the adsorption of N_2 at the temperature of liquid nitrogen (77 K). The BET surface area of the TD nanoparticles was 120 m^2/g and the BET surface area of P25 was 50 m^2/g. A larger surface area provides more surface active sites for the adsorption of reactive molecules, which leads the photocatalytic process to be more efficient [46].

3.2. MO photodecolorization

Photocatalytic decolorization of MO was experimented with P25, MNP, $nTiO_2$, TD, and MT, under UV light (λ = 254 nm). Decolorization kinetics was faster with P25, compared to the others. Interestingly, decolorization kinetic with TD was much faster than with MT while the two contain the same ratio of Fe and Ti. Photodecolorization with TD at different initial concentrations of MO is shown in Fig. 5(B). Almost complete decolorization was achieved within 180 min at 3.05×10^{-3}, 6.11×10^{-3}, and 9.16×10^{-3} mM of MO. MO decolorization with TD in this research can be adequately modeled with the Langmuir–Hinshelwood (L–H) kinetics, which takes into account the adsorption of the dye over the surface of TD, surface reaction, and desorption of products as shown in Fig. 5(C). The rate of reaction can be:

$$\frac{1}{r_0} = \frac{1}{k_{L-H}K_{ads}C_0} + \frac{1}{k_{L-H}} \quad (1)$$

where r_0 is the initial decolorization rate of MO (mg/L/min), k_{L-H} is the observed decolorization rate constant, K_{ads} is the adsorption coefficient of MO, and C_0 is initial MO concentration (mg/L). The parameters were determined from the slope and intercept of the linear fit of the $1/r_0$ vs. $1/C_0$ in Fig. 5(C). Calculated K_{ads} (L/mg) and k_{L-H} (mg/L/min) were 0.0812 and 0.0478, respectively. (Table 1).

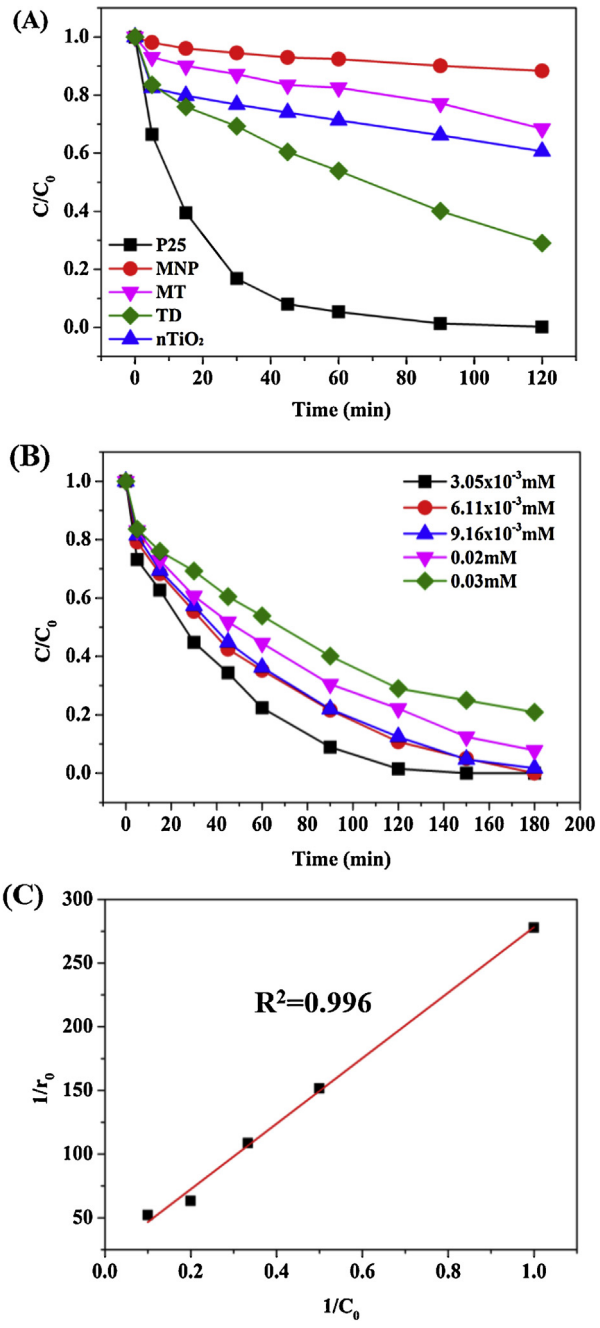

Fig. 5. (A) Photocatalytic decolorization of MO by P25, MNP, $nTiO_2$, TD, MT under UV light. (B) TD with different initial concentrations of MO (3.05×10^{-3}, 6.11×10^{-3}, 9.16×10^{-3}, 0.02 mM). (C) The Langmuir–Hinshelwood plot of MO photocatalytic decolorization of TD are shown.

Photocatalytic decolorization is initiated by photoexcitation of the semiconductor and formation of electron hole pairs on the surface of the catalysts. The pH decreased during UV irradiation because more NO_3^-, SO_4^{2-}, PO_4^{3-}, CO_2, and H_2O were produced with the reaction [47]. Optimal pH for the reaction between TiO_2

Table 1
Specific surface area of P25, $nTiO_2$, MT, and TD in this research.

	Specific surface area (m^2/g)	Crystallite size (nm)
P25	50	30
$nTiO_2$	6.56	6
MT	12.61	6–13
TD	120.02	20–25

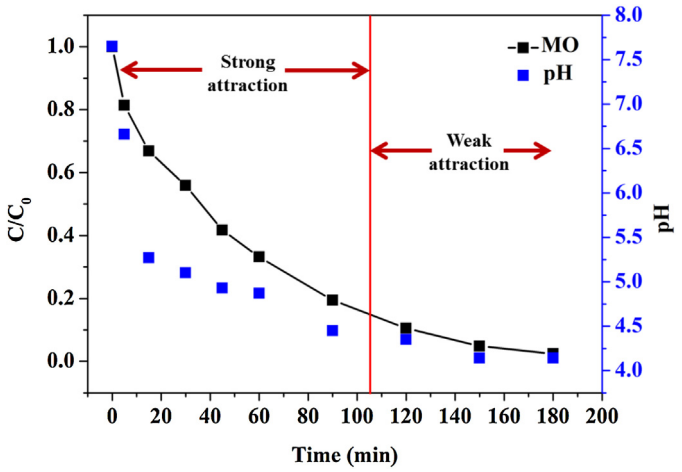

Fig. 6. Effect of pH on the decolorization of MO (3 mg/L) by TD.

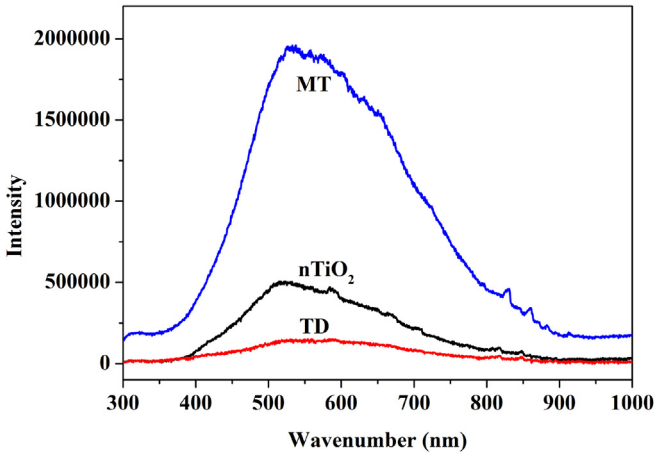

Fig. 7. Photoluminescence spectra of MT, $nTiO_2$, TD (λ_{ex} = 300 nm).

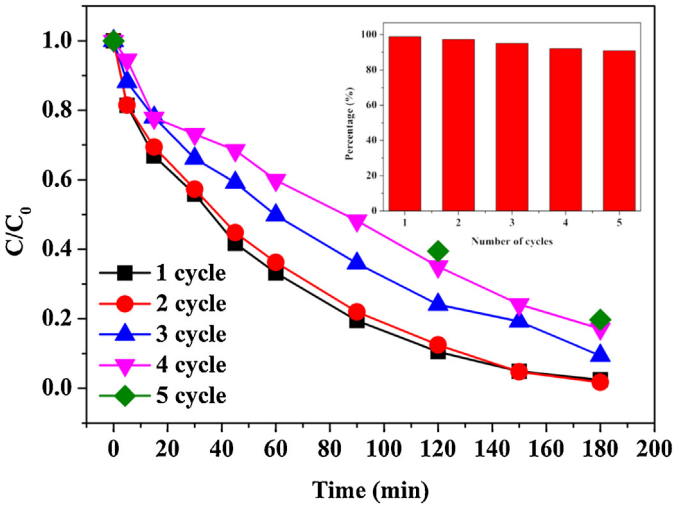

Fig. 8. Recycle and reuse of TD for M Recycle and reuse of TD for MO decolorization (MO concentration: 3 mg/L; TD dosage: 1 g/L; natural pH; irradiation time: 3 h).

and MO is reported as between 4.4 and 6.25 [48]. Strong electrostatic attraction between MO and TiO_2 was reported at pHs above 4.4 while weak attraction was monitored below at pHs less than 4.4 [48]. MO rapidly decreased for initial 120 min due to electrostatic attraction between MO and TiO_2 (Fig. 6). Photoexcitation in the semiconductor causes the formation of electron–hole pairs on the catalyst surface. When the $nTiO_2$ particles in TD are irradiated with UV having energy higher than its band gap energy, the electrons in the valence band are promoted to the conduction band. These photogenerated electrons are transferred to the polymer of TD, facilitating the hole–electron separation. Fluorescence emission of the P25, $nTiO_2$, MT, and TD was measured in ethanol. The intensity value was in the order of P25 > $nTiO_2$ > MT > TD. This fluorescence emission intensity is closely related with electron transfer process [49]. Excited electrons were rapidly transferred into polymeric structure of the TD and less recombination was observed with the TD. The recombination process occurs in the microsecond or sub-microsecond time scale. The fluorescence lifetimes are given in Table 2. Longer lifetime indicates a decrease in recombination rate [50]. Longer lifetime of the TD can be due to the TD dendritic branches. Photoluminescence emission spectra are useful to disclose the efficiency of charge carrier and to understand the fate of electron–hole pairs in semiconductor particles [51]. The effect of TD polymeric structure on the recombination of electron–hole pairs was further investigated with photoluminescence spectra of MT, $nTiO_2$, and TD at an excitation wavelength of 300 nm (Fig. 7). The TD exhibited much lower emission intensity than $nTiO_2$ and MT, implying that the recombination of photogenerated electrons and holes was greatly inhibited in TD. Photogenerated electrons of excited $nTiO_2$ could be transferred instantly from the conduction band of $nTiO_2$, resulting in an improved charge separation and consequently higher photocatalytic activity than $nTiO_2$ alone. Similarly, electron transfer between TiO_2 and polymers were observed in other systems [52,53].

Table 2
The fluorescence lifetime of P25, nTiO2, MT, MNP, and TD in this research.

	Excitation wavenumber (nm)	Emission wavenumber (nm)	Lifetime (μs)
MNP	293	325.9	40
MT	294	323	35
$nTiO_2$	297.1	324.9	30
P25	298.1	326.9	48
TD	293	321	68

Repetitive use is very important for the environmental sustainability of catalysts. Regeneration and recovery of TD were carried out five consecutive runs. Fig. 8 suggests that MO decolorization with TD was about 90%, which indicated that TD maintained similar photocatalytic activity after five times of recycling.

4. Conclusion

The TD catalysts were successfully synthesized with MD and $nTiO_2$. Synthesized TD could enhance MO adsorption and photodecolorization of MO compared to $nTiO_2$. Experimental results showed that polymer of TD role in electron capture. Furthermore, the polymer of TD prevents the recombination of holes with electrons of TiO_2, leading to the enhancement of photocatalytic activity for TD. Also, the TD of hybrid catalyst is conveniently recoverable due to the magnetic core. In summary, MD containing $nTiO_2$ functional groups exhibited restrained recombination electron–hole pairs and high performance UV irradiation responsive catalyst and it can be widely used as a photocatalyst in various applications, including water treatment.

Acknowledgments

This work was supported by Nano-Convergence Foundation [Synthesis of magnetic-cored dendrimer nano material for high

efficiency adsorption of heavy metal] funded by the Ministry of Education, Science and Technology (MEST, Korea) & the Ministry of Knowledge Economy (MKE, Korea), and by the Korea Ministry of Environment as "The GAIA Project (20120000550001).

References

[1] P. Lei, F. Wang, X. Gao, Y. Ding, S. Zhang, J. Zhao, S. Liu, M. Yang, Journal of Hazardous Materials 227–228 (2012) 185–194.
[2] Y. Yang, H. Wang, J. Li, B. He, T. Wang, S. Liao, Environmental Science & Technology 46 (2012) 6815–6821.
[3] B.Y. Yu, S.-Y. Kwak, Journal of Materials Chemistry 22 (2012) 8345–8353.
[4] Z. Zhang, Y. Xu, X. Ma, F. Li, D. Liu, Z. Chen, F. Zhang, D.D. Dionysiou, Journal of Hazardous Materials 209–210 (2012) 271–277.
[5] A. Charanpahari, S.S. Umare, S.P. Gokhale, V. Sudarsan, B. Sreedhar, R. Sasikala, Applied Catalysis A: General 443–444 (2012) 96–102.
[6] C. Sahoo, A.K. Gupta, Journal of Hazardous Materials 215–216 (2012) 302–310.
[7] P. Song, X. Zhang, M. Sun, X. Cui, Y. Lin, Nanoscale 4 (2012) 1800–1804.
[8] J.-W. Jang, J.-W. Park, Thin Solid Films 520 (2011) 193–198.
[9] D.D. Sun, P.F. Lee, Separation and Purification Technology 91 (2012) 30–37.
[10] H. Liu, Z. Jia, S. Ji, Y. Zheng, M. Li, H. Yang, Catalysis Today 175 (2011) 293–298.
[11] X. Hu, J. Yang, J. Zhang, Journal of Hazardous Materials 196 (2011) 220–227.
[12] T.A. Gad-Allah, K. Fujimura, S. Kato, S. Satokawa, T. Kojima, Journal of Hazardous Materials 154 (2008) 572–577.
[13] Y. Nakanishi, T. Imae, Journal of Colloid and Interface Science 285 (2005) 158–162.
[14] Y. Nakanishi, T. Imae, Journal of Colloid and Interface Science 297 (2006) 122–129.
[15] G.R. Newkome, C.N. Moorefield, F. Vogtle, Dendritic Molecules: Concepts, Syntheses Perspectives, Wiley-VCH, 1996.
[16] J.M.J. Frechet, D.A. Tomalia, Dendrimers and Other Dendritic Polymers, Wiley-VCH, 2001.
[17] A. Sarkar, P.I. Carver, T. Zhang, A. Merrington, K.J. Bruza, J.L. Rousseau, S.E. Keinath, P.R. Dvornic, Journal of Membrane Science 349 (2010) 421–428.
[18] D.A. Tomalia, A.M. Naylor, W.A. Goddard, Angewandte Chemie International Edition in English 29 (1990) 138–175.
[19] C.t. Ornelas, J. Broichhagen, M. Weck, Journal of the American Chemical Society 132 (2010) 3923–3931.
[20] M. Shen, X. Shi, Nanoscale 2 (2010) 1596–1610.
[21] S.H. Medina, V. Tekumalla, M.V. Chevliakov, D.S. Shewach, W.D. Ensminger, M.E.H. El-Sayed, Biomaterials 32 (2011) 4118–4129.
[22] A. Sharma, S.P. Gautam, A.K. Gupta, Bioorganic and Medicinal Chemistry 19 (2011) 3341–3346.
[23] M. Ciolkowski, J.F. Petersen, M. Ficker, A. Janaszewska, J.B. Christensen, B. Klajnert, M. Bryszewska, Nanomedicine: Nanotechnology, Biology and Medicine (2012).
[24] M.N. Luwang, S. Chandra, D. Bahadur, S.K. Srivastava, Journal of Materials Chemistry 22 (2012) 3395–3403.
[25] M.S. Diallo, L. Balogh, A. Shafagati, Johnson, H. James, W.A. Goddard, D.A. Tomalia, Environmental Science & Technology 33 (1999) 820–824.
[26] J.W. Jang, L.J. Kim, J.W. Park, 10th International Conference on Materials Chemistry, 2011.
[27] I.H. Yeo, J.Y. Yoo, J.W. Jang, J.W. Park, The Fourth IWA-ASPIRE Conference & Exhibition, 2011.
[28] R.V. Mehta, R.V. Upadhyay, S.W. Charles, C.N. Ramchand, Biotechnology Techniques 11 (1997) 493–496.
[29] C.-M. Chou, H.-L. Lien, Journal of Nanoparticle Research 13 (2011) 2099–2107.
[30] B. Pan, D. Cui, Y. Sheng, C. Ozkan, F. Gao, R. He, Q. Li, P. Xu, T. Huang, Cancer Research 67 (2007) 8156–8163.
[31] P. Periyat, S.C. Pillai, D.E. McCormack, J. Colreavy, S.J. Hinder, Journal of Physical Chemistry C 112 (2008) 7644–7652.
[32] M. Vettraino, M. Trudeau, D.M. Antonelli, Inorganic Chemistry 40 (2001) 2088–2095.
[33] H. Liu, H.T. Ma, X.Z. Li, W.Z. Li, M. Wu, X.H. Bao, Chemosphere 50 (2003) 39–46.
[34] F. Gao, B.-F. Pan, W.-M. Zheng, L.-M. Ao, H.-C. Gu, Journal of Magnetism and Magnetic Materials 293 (2005) 48–54.
[35] D. Wang, L. Xiao, Q. Luo, X. Li, J. An, Y. Duan, Journal of Hazardous Materials 192 (2011) 150–159.
[36] R. Li, J. Bu, Korean Journal of Chemical Engineering 21 (2004) 98–103.
[37] O.M. Mikhailik, O.M. Fedorenko, S.S. Mikhailova, V.I. Povstugar, A.M. Lyakhovich, G.T. Kurbatova, N.I. Shklovskaya, A.A. Chuiko, Colloids and Surfaces A: Physicochemical and Engineering Aspects 52 (1991) 331–338.
[38] K. Wapner, G. Grundmeier, Surface and Coatings Technology 200 (2005) 100–103.
[39] Z. Xu, Q. Liu, J.A. Finch, Applied Surface Science 120 (1997) 269–278.
[40] B.F. Pan, F. Gao, H.C. Gu, Journal of Colloid and Interface Science 284 (2005) 1–6.
[41] R. Qiu, D. Zhang, Z. Diao, X. Huang, C. He, J.-L. Morel, Y. Xiong, Water Research 46 (2012) 2299–2306.
[42] C. Chan, H. Gallard, P. Majewski, Journal of Nanoparticle Research 14 (2012) 1–11.
[43] D. Zhang, Z. Liu, S. Han, C. Li, B. Lei, M.P. Stewart, J.M. Tour, C. Zhou, Nano Letters 4 (2004) 2151–2155.
[44] A.A. Aziz, K.S. Yong, S. Ibrahim, S. Pichiah, Journal of Hazardous Materials 199–200 (2012) 143–150.
[45] D. Zhao, G. Sheng, C. Chen, X. Wang, Applied Catalysis B: Environmental 111–112 (2012) 303–308.
[46] J. Yu, W. Wang, B. Cheng, Chemistry—An Asian Journal 5 (2010) 2499–2506.
[47] J. Wang, B. Guo, X. Zhang, Z. Zhang, J. Han, J. Wu, Ultrasonics Sonochemistry 12 (2005) 331–337.
[48] L. Andronic, A. Duta, Materials Chemistry and Physics 112 (2008) 1078–1082.
[49] K.M. Rahulan, N. Padmanathan, G. Vinitha, C.C. Kanakam, Materials Research Bulletin 48 (2013) 3037–3042.
[50] M. Wang, H. Xie, J. Zhu, M. Xie, T. Li, Y. Li, Journal of Materials Science 42 (2007) 7678–7683.
[51] F.B. Li, X.Z. Li, Applied Catalysis A: General 228 (2002) 15–27.
[52] H.-c. Liang, X.-z. Li, Applied Catalysis B: Environmental 86 (2009) 8–17.
[53] H. Zhang, X. Lv, Y. Li, Y. Wang, J. Li, ACS Nano 4 (2009) 380–386.